

Doped Valence-bond Solid and Superconductivity on the Shastry-Sutherland Lattice

Bohm-Jung Yang,¹ Yong Baek Kim,^{2,3} Jaejun Yu,¹ and Kwon Park^{3,*}

¹*Department of Physics and Astronomy, Center for Strongly Correlated Materials Research, and Center for Theoretical Physics, Seoul National University, Seoul 151-747, Korea*

²*Department of Physics, University of Toronto, Toronto, Ontario M5S 1A7, Canada*

³*School of Physics, Korea Institute for Advanced Study, Seoul 130-722, Korea*

(Dated: October 25, 2018)

Motivated by recent experiments on $\text{SrCu}_2(\text{BO}_3)_2$, we investigate the ground states of the doped Mott insulator on the Shastry-Sutherland lattice. To provide a unified theoretical framework for both the valence-bond solid state found in undoped $\text{SrCu}_2(\text{BO}_3)_2$ and the doped counterpart being pursued in on-going experiments, we analyze the t - J - V model via the bond operator formulation. It is found that novel superconducting states emerge upon doping with their properties crucially depending on the underlying valence bond order. Implications to future experiments are discussed.

PACS numbers: 74.20.Mn, 74.25.Dw

I. INTRODUCTION

The fate of doped Mott insulators is one of the most challenging issues in correlated electron physics, especially in relation to the long-standing problem of high-temperature superconductivity in cuprates^{1,2,3}. Recent discoveries of various Mott insulators on geometrically frustrated lattices^{4,5,6,7} and organic materials⁸ may offer an important clue to this issue when such materials are doped. While it is possible that the ground state does not break any symmetry, resulting in a spin liquid phase, the ground states of Mott insulators often have broken spin-rotation and lattice-translation symmetries, leading to antiferromagnetic and valence bond solid order, respectively¹. Since both antiferromagnetic and valence bond solid phases are generic possibilities for Mott insulators, a zero-temperature quantum phase transition may occur between these two phases when an appropriate ‘‘control parameter’’ is changed¹. In this context, understanding the effect of doping on valence-bond solid phases is as equally important as that on antiferromagnetic phases and would be quite useful for the full classification of all possible phases of doped Mott insulators.

There are, however, not many clear examples of two-dimensional valence-bond solid insulator in contrast to the antiferromagnetic insulator found in high T_c cuprate compounds. The discovery of $\text{SrCu}_2(\text{BO}_3)_2$ is particularly important in this regard^{4,9,10}. This material can be characterized by an antiferromagnetic spin-1/2 Heisenberg model on the Shastry-Sutherland lattice¹¹. Starting from the usual square lattice, the Shastry-Sutherland lattice can be obtained by putting additional diagonal bonds with two possible orientations in alternating plaquettes (see Fig.1). Let J and J' be the exchange couplings along the diagonal and the square lattice links, respectively. It is known that the valence bond solid state or the product state of valence bond singlets (illustrated as filled ellipses in Fig.1) along the diagonal bonds is the exact ground state of the Heisenberg model for $J'/J < 0.7$ ^{11,12,13,14,15,16,17,18}. In $\text{SrCu}_2(\text{BO}_3)_2$, J'/J is estimated to be 0.64⁴.

In this paper, we investigate possible phases of doped

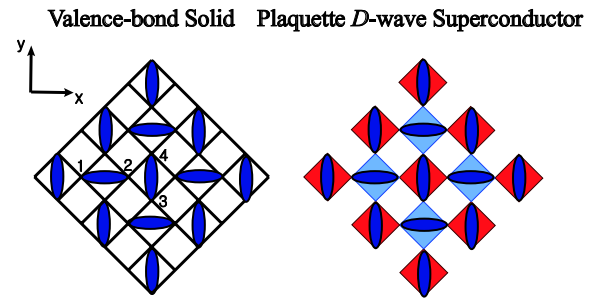


FIG. 1: (Color online) Schematic diagram for the ground states on the Shastry-Sutherland lattice. The valence-bond solid state is the ground state at half filling as depicted in the left figure where ellipses represent spin-singlet pairs. When doped with holes, the system exhibits superconductivity in addition to the coexisting valence-bond solid order. Furthermore, when the nearest-neighbor repulsive interaction, V , is larger than a critical value, V_c , the plaquette D -wave superconductivity appears in a range of doping concentration, x , with a peculiar spatial pattern as shown in the right figure. In this situation, the pairing amplitudes residing in the four links encircling the horizontal dimers have the opposite sign to those for the vertical dimers. Different colors are used to emphasize the plaquette pattern of the pairing amplitude.

valence-bond solid and superconductivity on the Shastry-Sutherland lattice. In order to study the interplay between the valence-bond solid order and emergent superconductivity at finite doping, we use the bond operator formulation^{19,20,21} of the constrained Hilbert space of correlated electron systems, extended to general doping and applied to the t - J - V model. Here t and V represent the hopping strength and nearest-neighbor repulsion between electrons, respectively. In contrast to previous studies of the Shastry-Sutherland model^{23,24,25}, the emergent superconducting state is directly related to the underlying valence-bond solid order at the half-filling. For example, the valence-bond solid order is so robust that superconductivity always coexists with it as shown in the resulting phase diagram of Fig. 2.

When the nearest-neighbor repulsion, V , is smaller than a critical value V_c , the doped holes can remain paired mostly

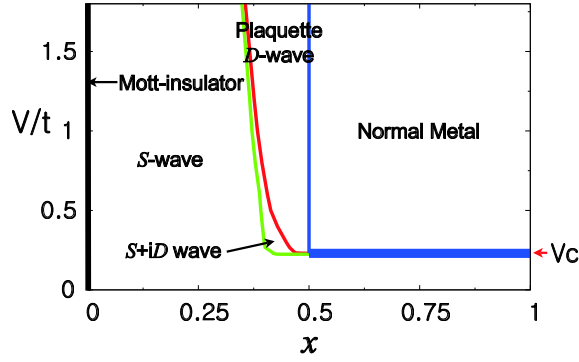


FIG. 2: (Color online) Phase diagram of the t - J - V model on the Shastry-Sutherland lattice as a function of hole concentration, x , and the nearest-neighbor repulsive interaction, V . The thick line separating the normal metal and the S -wave superconducting phase is a first-order phase boundary, while other boundaries are all second-order. The undoped Mott-insulating state is represented by the thick solid line at $x = 0$.

within each valence-bond singlet or dimer on the diagonal bonds. This leads to S -wave superconductivity. On the other hand, when V is larger than V_c , the Coulomb repulsion prevents doped holes from occupying the same dimer. At larger doping concentrations, the doped holes tend to develop pairing correlation between nearby dimers of the valence-bond singlets. Consequently the superconducting order parameter acquires an interesting phase relation on the square lattice link, depending on whether the square lattice links encircle the horizontal or vertical dimers (See Fig. 1). More specifically, all the links within the same plaquette have the same sign, but those in the nearest-neighbor plaquettes have the opposite sign. Since this looks like D -wave symmetry at long distances, we call it the *plaquette* D -wave superconductivity. Notice, however, that this is different from the ordinary d -wave superconductor on the square lattice where the sign alternates for different links within the same plaquette. This peculiar structure comes from the underlying valence bond solid order. The simultaneous presence of the valence bond order and superconductivity can, in principle, be checked by X-ray or neutron scattering experiments.

The rest of the paper is organized as follows. In section II, we review the bond operator formulation for doped magnets. In section III, the t - J - V Hamiltonian is written in the bond operator representation and the mean field theory is explained. In section IV, the results of the mean field theory and the phase diagram are discussed. We conclude in section V. Some details of the computations are relegated to the appendix.

II. BOND OPERATOR FORMALISM

We start with the bond operator theory by setting up an exact mapping between bond operators and usual electron creation operators^{19,20,21}. Let c_{1a}^\dagger and c_{2a}^\dagger ($a = \uparrow, \downarrow$) be the electron creation operators on the left and right site, respectively,

of the lattice link that a horizontal dimer occupies (see Fig. 1). In the limit of large on-site repulsive interaction, U , any state with two electrons at the same site is excluded from the low-energy Hilbert space which in turn can be represented by nine “bond-particle” creation operators defined as follows:

- (i) Singlet boson for spin-Peierls order,

$$s^\dagger|v\rangle = \frac{1}{\sqrt{2}}\varepsilon_{ab}c_{1a}^\dagger c_{2b}^\dagger|0\rangle, \quad (1)$$

where $|0\rangle$ is the electron vacuum and $|v\rangle$ is the imaginary vacuum void of any bond particle. ε_{ab} is the second-rank antisymmetric tensor with $\varepsilon_{\uparrow\downarrow} = 1$. From now on we adopt the summation convention for repeated spin indices (such as a and b above) throughout this paper unless mentioned otherwise.

- (ii) Triplet magnon,

$$t_\alpha^\dagger|v\rangle = \frac{1}{\sqrt{2}}\sigma_{bc}^\alpha\varepsilon_{ca}c_{1a}^\dagger c_{2b}^\dagger|0\rangle, \quad (2)$$

where σ_{ab}^α ($\alpha = x, y, z$) are the usual Pauli matrices.

- (iii) Single-hole fermion,

$$\begin{aligned} h_{1a}^\dagger|v\rangle &= c_{1a}^\dagger|0\rangle, \\ h_{2a}^\dagger|v\rangle &= c_{2a}^\dagger|0\rangle. \end{aligned} \quad (3)$$

- (iv) Double-hole boson for the empty state,

$$d^\dagger|v\rangle = |0\rangle. \quad (4)$$

As indicated by the names, the operators s , d , and t_α all obey the canonical boson commutation relations while h_{1a} and h_{2a} satisfy the canonical fermion anticommutation relations. To eliminate unphysical states from the enlarged Hilbert space, the following constraint needs to be imposed on the bond-particle Hilbert space:

$$s^\dagger s + t_\alpha^\dagger t_\alpha + h_{1a}^\dagger h_{1a} + h_{2a}^\dagger h_{2a} + d^\dagger d = 1. \quad (5)$$

Constrained by this equation, the exact expressions for the spin and electron creation operators can be written in terms of the bond operators. For example,

$$\begin{aligned} S_{1\alpha} &= \frac{1}{2}(s^\dagger t_\alpha + t_\alpha^\dagger s - i\varepsilon_{\alpha\beta\gamma}t_\beta^\dagger t_\gamma) + \frac{1}{2}\sigma_{ab}^\alpha h_{1a}^\dagger h_{1b}, \\ S_{2\alpha} &= -\frac{1}{2}(s^\dagger t_\alpha + t_\alpha^\dagger s + i\varepsilon_{\alpha\beta\gamma}t_\beta^\dagger t_\gamma) + \frac{1}{2}\sigma_{ab}^\alpha h_{2a}^\dagger h_{2b}, \\ c_{1a}^\dagger &= h_{1a}^\dagger d + \frac{1}{\sqrt{2}}\varepsilon_{ab}s^\dagger h_{2b} - \frac{1}{\sqrt{2}}\varepsilon_{ac}\sigma_{cb}^\alpha t_\alpha^\dagger h_{2b}, \\ c_{2a}^\dagger &= h_{2a}^\dagger d + \frac{1}{\sqrt{2}}\varepsilon_{ab}s^\dagger h_{1b} + \frac{1}{\sqrt{2}}\varepsilon_{ac}\sigma_{cb}^\alpha t_\alpha^\dagger h_{1b}, \end{aligned} \quad (6)$$

where $\varepsilon_{\alpha\beta\gamma}$ is the third rank antisymmetric tensor with $\varepsilon_{xyz} = 1$.

Now, in order to cover the full Shastry-Sutherland lattice, we need nine additional bond operators representing the electronic Hilbert space associated with the vertical dimers corresponding to the sites 3 and 4. For example, τ_α indicates the triplet magnon in the vertical dimers while h_{3a} and

h_{4a} represent the corresponding single-hole fermions. While non-uniform condensations of the spin-Peierls singlet and/or double-hole bosons are in general possible, we focus only on the uniform phases in this study. Thus the condensation densities of the singlet and double-hole bosons will be represented by \bar{s} and \bar{d} for both horizontal and vertical dimers.

III. CHOICE OF HAMILTONIAN AND BOND OPERATOR MEAN FIELD THEORY

We consider the following t - J - V Hamiltonian:

$$H = \hat{P}_G \left[- \sum_{\langle i,j \rangle} t_{ij} (c_{ia}^\dagger c_{ja} + \text{H. c.}) - \mu \sum_i c_{ia}^\dagger c_{ia} + \sum_{\langle i,j \rangle} J_{ij} \mathbf{S}_i \cdot \mathbf{S}_j + \sum_{\langle i,j \rangle} V_{ij} n_i n_j \right] \hat{P}_G, \quad (7)$$

where \hat{P}_G is the Gutzwiller projection operator imposing the no-double-occupancy constraint. t_{ij} and J_{ij} are the electron hopping matrix element and antiferromagnetic exchange interaction, respectively. In this paper, we set $t_{ij} = t$ and $J_{ij} = J$ within a dimer, $t_{ij} = t'$ and $J_{ij} = J'$ between neighboring dimers. We take $J'/J = 0.64$ from the experiments on $\text{SrCu}_2(\text{BO}_3)_2$ ^{4,23}. From the large- U expansion of the Hubbard model, we can then set $t'/t = \sqrt{J'/J} = 0.8$. However, the parameter, J'/t' , which is important for hole dynamics, is not available experimentally. Thus we follow the convention used in previous works²³ and take $J'/t' = 0.3$. Also, μ is the chemical potential and n_i is the electron density operator. Finally, for convenience, the nearest-neighbor repulsive interaction, V_{ij} , is set to V for both the two sites within dimer and those between the nearest-neighbor dimers.

We now write the t - J - V Hamiltonian solely in terms of the bond particle operators¹⁹. As usual, the constraint on the bond particle operators is imposed by the Lagrange multiplier method. Residual interactions between bond particles are analyzed via quadratic decoupling of quartic terms in a similar manner to the usual Hartree-Fock-BCS treatment. For the mean-field description, we consider the following order parameters:

$$\begin{aligned} P_x &\equiv \langle t_{i\alpha}^\dagger \tau_{i+\hat{x},\alpha} \rangle, \quad Q_x \equiv \langle t_{i\alpha} \tau_{i+\hat{x},\alpha} \rangle, \\ \Pi_x &= \langle h_{1i\alpha}^\dagger h_{3,i-\hat{x},a} \rangle = \langle h_{1i\alpha}^\dagger h_{4,i-\hat{x},a} \rangle \\ &= \langle h_{2i\alpha}^\dagger h_{3,i+\hat{x},a} \rangle = \langle h_{2i\alpha}^\dagger h_{4,i+\hat{x},a} \rangle, \\ \Delta_x &= \langle h_{1i\downarrow} h_{3,i-\hat{x},\uparrow} \rangle = \langle h_{1i\downarrow} h_{4,i-\hat{x},\uparrow} \rangle \\ &= \langle h_{2i\downarrow} h_{3,i+\hat{x},\uparrow} \rangle = \langle h_{2i\downarrow} h_{4,i+\hat{x},\uparrow} \rangle, \end{aligned} \quad (8)$$

where \mathbf{i} is the dimer index of the horizontal dimers and $\mathbf{i} \pm \hat{x}$ indicates the locations of the neighboring vertical dimers. The order parameters for the y -direction can be defined similarly.

We consider the possibility that the valence-bond-solid order persists even at non-zero doping. We further consider the condensation of d bosons, but neglect the possibility of triplet condensation because we are mostly concerned about paramagnetic phases in this work. All of the order parameters (P , Q ,

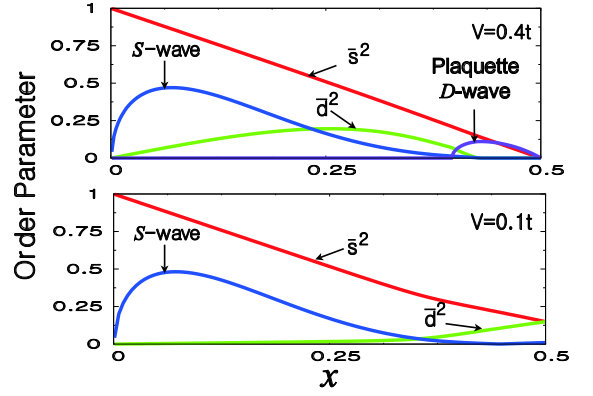


FIG. 3: (Color online) Superconducting order parameter, χ , as well as condensation densities of the spin-Peierls singlets, \bar{s} , and double-hole bosons, \bar{d} , as a function of hole concentration, x . When $V = 0.4t > V_c$ (top panel), S -wave χ and \bar{d} simultaneously vanish at $x = 0.431$. Before the full plaquette D -wave superconductivity sets in at larger x , there is a region, $0.389 < x < 0.431$, where the S - and D -wave superconductivity coexists in the form of $S+iD$ -wave. Finally at $x = 0.5$, the plaquette D -wave superconducting order parameter becomes zero and so does \bar{s} . No valence-bond solid correlation exists for $x \geq 0.5$. When $V = 0.1t < V_c$ (bottom panel), \bar{d} increases monotonically as a function of x while \bar{s} remains finite all the way to $x = 1$. For clarity the S - and plaquette D -wave superconducting order parameters as well as \bar{d}^2 are magnified twenty times in the top panel while, in the bottom panel, only the S -wave superconducting order parameter is magnified twenty times.

Π , and Δ for both x and y directions) defined above as well as \bar{s} , \bar{d} , the chemical potential, μ , and the Lagrange multiplier, ξ , are determined by solving a coupled set of four saddle-point equations and eight self-consistency equations. Details of the computational procedure are presented in the Appendix.

IV. RESULTS OF THE MEAN FIELD THEORY AND THE PHASE DIAGRAM

At zero doping, the system is in a robust valence-bond solid phase. In our bond operator theory, the robustness of the ground state can be seen by the complete localization of triplet magnons: the t_α and τ_α dispersions are completely flat and high in energy. It can easily be shown that, at the quadratic order, the triplet magnons on the Shastry-Sutherland lattice are completely decoupled from the singlet contributions (Notice that the coupling between the singlets and triplets at the quadratic order were the main driving force for the triplet dispersion in the square-lattice case¹⁹). This leads to the triplet Hamiltonian with no dispersive quadratic part. Thus, the only way to generate the triplet dispersion is through the saddle-point order parameters, P_x, P_y, Q_x and Q_y . It turns out, however, that all of the above order parameters are actually zero for any J'/J at half filling in our mean-field theory so that the triplets are completely localized.

Now let us consider the case of non-zero doping. In our Hartree-Fock-BCS saddle-point approximation, superconduc-

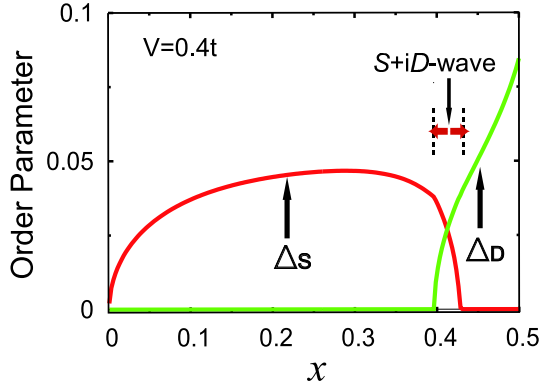


FIG. 4: h -fermion pairing amplitude, Δ , as a function of hole concentration, x . In the plot, Δ_S and Δ_D indicate the S - and D -wave components of Δ , respectively. Note that there is a region, $0.389 < x < 0.431$, where the S - and D -wave superconductivity coexist in the form of the $S+iD$ -wave.

tivity is found to appear at any non-zero doping when one neglects long-range charge inhomogeneities such as Wigner crystal order at very small x . In the bond operator representation, the electron superconducting order parameter can be computed from

$$\begin{aligned} \chi_x &= \varepsilon_{ab} \langle c_{11a}^\dagger c_{3,i-\hat{x},b}^\dagger \rangle = \varepsilon_{ab} \langle c_{11a}^\dagger c_{4,i-\hat{x},b}^\dagger \rangle \\ &= \varepsilon_{ab} \langle c_{21a}^\dagger c_{3,i+\hat{x},b}^\dagger \rangle = \varepsilon_{ab} \langle c_{21a}^\dagger c_{4,i+\hat{x},b}^\dagger \rangle \\ &= (2\bar{d}^2 - \bar{s}^2 - Q_x) \Delta_x - \sqrt{2} \bar{s} \bar{d} \Pi_x. \end{aligned} \quad (9)$$

The superconducting order parameter for the y -direction is defined similarly. The doping dependence of χ is plotted in Fig. 3 along with the singlet boson condensate density, \bar{s} , and the double-hole boson condensate density, \bar{d} .

While χ can be a complex number in general, it turns out to be real for most of the phase space, barring an arbitrary overall phase factor (See Fig. 2). In Fig. 2, however, there is a narrow region where the S - and D -wave superconductivity coexists in the form of an $S+iD$ -state similar to the results of previous studies on the square lattice²⁸. In this case χ_x is a complex number and $\chi_x = \chi_y^*$. As shown in Eq. (9), the h -fermion pairing amplitude, Δ , is the key element in determining the sign of χ and thereby the pairing symmetry of the electronic superconducting order parameter. Generally the momentum dependence of Δ can be written as follows:

$$\begin{aligned} \Delta_{S+iD} &= \Delta_x \cos k_x + \Delta_y \cos k_y \\ &= \Delta e^{i\varphi} \cos k_x + \Delta e^{-i\varphi} \cos k_y \\ &\equiv \Delta_S (\cos k_x + \cos k_y) + i \Delta_D (\cos k_x - \cos k_y). \end{aligned} \quad (10)$$

If both Δ_S and Δ_D remain finite, the system possesses the $S+iD$ -wave pairing symmetry. In Fig. 4 we plot the detailed doping dependence of Δ_S and Δ_D for $V = 0.4t$.

Notice that the critical exponent, β , defined in $\chi \sim |x - x_c|^\beta$ shows an interesting behavior when $V > V_c$. Superconducting order parameters for both S - and D -wave show the usual mean-field behavior, i.e., $\beta = 1/2$, when they first

emerge. On the other hand, when they disappear, both exhibit an unusual exponent of $\beta = 1$. This deviation from the conventional mean-field behavior has different origins in each case. For the S -wave case, the phase boundary corresponds to the critical point between $S+iD$ -wave and D -wave superconductivity, where the presence of nodal fermions leads to a non-analytic cubic term in the expansion of the ground state energy^{26,27}. On the other hand, for the D -wave, the linearly vanishing \bar{s}^2 gives rise to $\beta = 1$ (Note that Δ_D remains finite at the critical point $x = 0.5$. See Fig. 4).

It is also interesting to note that our h -fermion (defined on a dimer) is an extended object which carries both the charge and spin quantum numbers. As a consequence, when the h -fermion pairing amplitude is finite, the distance between two holes in a h - h pair is larger than the average electron distance, as reported in exact diagonalization studies²⁹. This behavior is different from what one would expect in the slave-boson-type theory^{23,24}.

In Fig. 2 the zero-temperature phase diagram is plotted as a function of hole concentration, x , and the nearest-neighbor repulsive interaction, V . The overall shape of the phase diagram is determined by the behavior of the d -boson condensate, which corresponds to the local pairing of holes within dimers. For $V < V_c \simeq 0.23t$, the d -boson condensation is the primary mechanism of pairing and its short-range nature generates S -wave pairing rather than D -wave with a nodal structure. On the other hand, for $V > V_c$, there is a V -dependent critical hole concentration, x_c , where \bar{d} vanishes. It is this collapse of d -boson condensates that makes pairing more long-ranged and finally leads to the emergence of D -wave superconductivity.

The detailed x -dependence of the superconducting order parameter, χ , is shown in Fig. 3. For $V = 0.4t > V_c$, the S -wave superconducting order parameter and the d -boson condensate density go to zero simultaneously at $x \simeq 0.431$. The collapse of the d -boson condensate at finite doping, in turn, imposes a precise upper bound on the hole concentration, up to which the valence-bond order can exist. To see this, note that, in the bond-operator representation, the chemical potential, μ , is fixed to satisfy $\langle h_{11a}^\dagger h_{11a} + h_{21a}^\dagger h_{21a} \rangle + 2\bar{d}^2 = 2x$. A similar equation exists for h_3 and h_4 fermions. When $\bar{d}^2 = 0$, hole doping can be achieved only through h -fermions. In this situation, the hole concentration cannot exceed $x = 1/2$ where every dimer has exactly one electron. Note that, for $V = 0.1t < V_c$, \bar{d}^2 increases monotonically as x increases and finally reaches unity at $x = 1$.

The plaquette D -wave superconducting order parameter found here has a peculiar spatial pattern as shown in Fig. 1. As explained in the introduction, this pattern is completely different from the corresponding pattern of the conventional d -wave superconducting state that previous slave-boson theories would predict^{23,24}. We argue that the order parameter pattern of our D -wave state is rather natural in the limit of strong dimerization. In this limit, two electrons within the same dimer lose their independent local coordinates and share the same single dimer index. Then, the links of the plaquette enclosing the horizontal (vertical) dimers would connect only the links of the nearest-neighbor plaquettes that encircle the

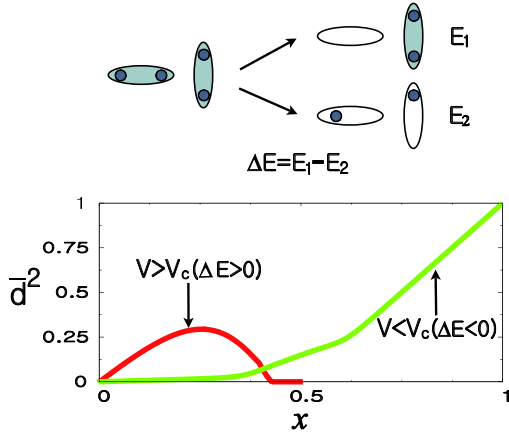


FIG. 5: (Color online) Schematic diagram showing the origin of different behaviors of the d boson condensate density below and above $V_c \simeq 0.23t$. The bottom figure plots \bar{d}^2 as a function of hole concentration, x , for $V = 0.4t$ ($\Delta E > 0$) and $V = 0.1t$ ($\Delta E < 0$). Note that for clarity \bar{d}^2 is magnified thirty times in the case of $V = 0.4t$.

vertical (horizontal) dimers. Thus it is natural to expect the plaquette-dependent order parameter.

Completely different behaviors of the d -boson condensate density below and above V_c can physically be understood as follows. When two holes are doped into a unit cell, there are two possible configurations as shown in Fig. 5. First, two electrons are removed from the same dimer while the other remains intact. In this case, only one singlet pair is removed, which costs the energy of $E_1 = E_s \sim J$ with an additional Coulomb energy gain due to the disappearance of nearest-neighbor electrons: $E_d \sim V$. Thus the total energy cost would be $E_1 = E_s - E_d \sim J - V$. Second, when two electrons are removed from two dimers, i.e., one hole remains at each dimer, there are twice the Coulomb energy gain and twice the exchange energy cost for breaking two singlet pairs. The total energy cost for the second case is $E_2 \sim 2E_1$. In conclusion, the energy-cost difference between two configurations is $\Delta E = E_1 - E_2 \sim V - J$. If $\Delta E < 0$, the first configuration is preferred and the d bosons can condense. On the other hand, if $\Delta E > 0$, the second configuration is favored and the d bosons may not condense depending on x , which is precisely the case as shown in the bottom figure of Fig. 5.

V. CONCLUSION

By analyzing the t - J - V model based on the bond operator formalism, we have investigated the phase diagram of the doped Mott insulator on the Shastry-Sutherland lattice. The interplay between strong dimerization and nearest-neighbor repulsive interactions leads to different behaviors of the doped holes determining the overall phase diagram. If the nearest-neighbor repulsive interaction, V , is smaller than a critical value, V_c , the hole-pairing within dimers is preferred, resulting in S -wave superconductivity at any non-zero x . On the other hand, if V is larger than V_c , the density of paired-holes

within the same dimers vanishes at finite x and the plaquette D -wave superconductivity with a peculiar spatial pattern emerges.

Considering clear experimental evidence for the valence-bond solid state in undoped $\text{SrCu}_2(\text{BO}_3)_2$, we believe that the above conclusions would be valid for a range of realistic situations. It will be interesting to observe the possible transition between the S - and D -wave superconducting states. Finally we note that, while doping mobile carriers to $\text{SrCu}_2(\text{BO}_3)_2$ has not been achieved yet, there has been a recent progress in doping quenched non-magnetic Mg impurities to this material³⁰.

This work was supported by the NSERC, CRC, CIAR, KRF-2005-070-C00044 (YBK) and by the KOSEF through CSCMR SRC (BJY, JY).

APPENDIX A: COMPUTATIONAL DETAILS

Here we present details of the Hartree-Fock-BCS mean field theory in the bond operator formalism. We begin by explicitly writing the t - J - V Hamiltonian as follows:

$$H = \hat{P}_G (H_t + H_J + H_\mu + H_V) \hat{P}_G, \quad (\text{A1})$$

where

$$\begin{aligned} H_t = & -t \sum_i (c_{1ia}^\dagger c_{2ia} + c_{3ia}^\dagger c_{4ia} + \text{H. c.}) \\ & - t' \sum_i \left[c_{1ia}^\dagger (c_{3,i-\hat{x},a} + c_{4,i-\hat{x},a}) \right. \\ & \quad \left. + c_{2ia}^\dagger (c_{3,i+\hat{x},a} + c_{4,i+\hat{x},a}) + \text{H. c.} \right] \\ & - t' \sum_i \left[c_{4ia}^\dagger (c_{1,i+\hat{y},a} + c_{2,i+\hat{y},a}) \right. \\ & \quad \left. + c_{3ia}^\dagger (c_{1,i-\hat{y},a} + c_{2,i-\hat{y},a}) + \text{H. c.} \right], \quad (\text{A2}) \end{aligned}$$

$$\begin{aligned} H_J = & J \sum_i (\mathbf{S}_{1i} \cdot \mathbf{S}_{2i} + \mathbf{S}_{3i} \cdot \mathbf{S}_{4i}) \\ & + J' \sum_i \left[\mathbf{S}_{1i} \cdot (\mathbf{S}_{3,i-\hat{x}} + \mathbf{S}_{4,i-\hat{x}}) + \mathbf{S}_{2i} \cdot (\mathbf{S}_{3,i+\hat{x}} + \mathbf{S}_{4,i+\hat{x}}) \right] \\ & + J' \sum_i \left[\mathbf{S}_{4i} \cdot (\mathbf{S}_{1,i+\hat{y}} + \mathbf{S}_{2,i+\hat{y}}) + \mathbf{S}_{3i} \cdot (\mathbf{S}_{1,i-\hat{y}} + \mathbf{S}_{2,i-\hat{y}}) \right], \quad (\text{A3}) \end{aligned}$$

$$\begin{aligned} H_\mu = & -\mu \sum_i (n_{1i} + n_{2i} - 2 + 2x) \\ & - \mu \sum_i (n_{3i} + n_{4i} - 2 + 2x), \quad (\text{A4}) \end{aligned}$$

and

$$\begin{aligned}
H_V &= V \sum_i (n_{1i}n_{2i} + n_{3i}n_{4i}) \\
&+ V \sum_i \left[n_{1i}(n_{3,i-\hat{x}} + n_{4,i-\hat{x}}) + n_{2i}(n_{3,i+\hat{x}} + n_{4,i+\hat{x}}) \right] \\
&+ V \sum_i \left[n_{4i}(n_{1,i+\hat{y}} + n_{2,i+\hat{y}}) + n_{3i}(n_{1,i-\hat{y}} + n_{2,i-\hat{y}}) \right].
\end{aligned} \tag{A5}$$

In the next section, the t - J - V Hamiltonian is expressed solely in terms of bond particles.

1. Hamiltonian in the bond-operator representation

Taking usual steps in any saddle-point theory, we first replace the full Gutzwiller projection by adding the Lagrange multiplier term. In the bond operator representation, this Lagrange multiplier term is written as follows:

$$\begin{aligned}
H_\xi &= -\xi \sum_i (s_i^\dagger s_i + t_{i\alpha}^\dagger t_{i\alpha} + h_{1ia}^\dagger h_{1ia} + h_{2ia}^\dagger h_{2ia} + d_i^\dagger d_i - 1) \\
&- \xi \sum_i (\sigma_i^\dagger \sigma_i + \tau_{i\alpha}^\dagger \tau_{i\alpha} + h_{3ia}^\dagger h_{3ia} + h_{4ia}^\dagger h_{4ia} + \delta_i^\dagger \delta_i - 1),
\end{aligned} \tag{A6}$$

where ξ is the Lagrange multiplier. Also, σ_i and δ_i represent the singlet boson and double-hole boson operators for the i -th vertical dimer, respectively. Other operators are defined in the main text. Under the constraint imposed by Eq. (A6), the usual chemical potential term can be written as follows:

$$\begin{aligned}
H_\mu &= \mu \sum_i (h_{1ia}^\dagger h_{1ia} + h_{2ia}^\dagger h_{2ia} + 2d_i^\dagger d_i - 2x) \\
&+ \mu \sum_i (h_{3ia}^\dagger h_{3ia} + h_{4ia}^\dagger h_{4ia} + 2\delta_i^\dagger \delta_i - 2x).
\end{aligned} \tag{A7}$$

Since we focus only on the phases with homogeneous singlet boson and double-hole boson condensates, from now on we set $s_i = s_i^\dagger = \bar{s}$, $\sigma_i = \sigma_i^\dagger = \bar{\sigma}$ and $d_i = d_i^\dagger = \bar{d}$, $\delta_i = \delta_i^\dagger = \bar{\delta}$. Furthermore, we neglect the possibility of triplet condensation in this paper.

By applying the bond operator representation to all the remaining terms in the Hamiltonian, the saddle-point Hamiltonian can be written as follows:

$$H = N\epsilon_0 + H_{\text{triplet}} + H_{\text{fermion}}, \tag{A8}$$

where the triplet boson Hamiltonian is given by

$$\begin{aligned}
H_{\text{triplet}} &= \sum_{\mathbf{k}} A_{\mathbf{k}} [t_\alpha^\dagger(\mathbf{k})\tau_\alpha(\mathbf{k}) + \tau_\alpha^\dagger(\mathbf{k})t_\alpha(\mathbf{k})] \\
&+ \sum_{\mathbf{k}} B_{\mathbf{k}} [t_\alpha^\dagger(\mathbf{k})\tau_\alpha^\dagger(-\mathbf{k}) + \tau_\alpha(-\mathbf{k})t_\alpha(\mathbf{k})] \\
&+ \sum_{\mathbf{k}} C_{\mathbf{k}} [t_\alpha^\dagger(\mathbf{k})t_\alpha(\mathbf{k}) + \tau_\alpha^\dagger(\mathbf{k})\tau_\alpha(\mathbf{k})],
\end{aligned} \tag{A9}$$

and the single-hole fermion Hamiltonian is given by

$$H_{\text{fermion}} = H_{\text{fermion}}^{(0)} + H_{\text{fermion}}^{\text{interaction}}, \tag{A10}$$

where

$$\begin{aligned}
H_{\text{fermion}}^{(0)} &= \sum_{\mathbf{k}} \left\{ a_{\mathbf{k}} [h_{1a}^\dagger(\mathbf{k})h_{2a}(\mathbf{k}) + h_{3a}^\dagger(\mathbf{k})h_{4a}(\mathbf{k})] + \text{H. c.} \right\} \\
&+ \sum_{\mathbf{k}} b_{\mathbf{k}} \left[h_{1a}^\dagger(\mathbf{k})h_{1a}(\mathbf{k}) + h_{2a}^\dagger(\mathbf{k})h_{2a}(\mathbf{k}) \right. \\
&\quad \left. + h_{3a}^\dagger(\mathbf{k})h_{3a}(\mathbf{k}) + h_{4a}^\dagger(\mathbf{k})h_{4a}(\mathbf{k}) \right],
\end{aligned} \tag{A11}$$

and

$$\begin{aligned}
H_{\text{fermion}}^{\text{interaction}} &= \sum_{\mathbf{k}} \left\{ c_{\mathbf{k}} [h_{3a}^\dagger(\mathbf{k})h_{1a}(\mathbf{k}) + h_{2a}^\dagger(\mathbf{k})h_{4a}(\mathbf{k})] + \text{H. c.} \right\} \\
&+ \sum_{\mathbf{k}} \left\{ d_{\mathbf{k}} [h_{4a}^\dagger(\mathbf{k})h_{1a}(\mathbf{k}) + h_{2a}^\dagger(\mathbf{k})h_{3a}(\mathbf{k})] + \text{H. c.} \right\} \\
&+ \sum_{\mathbf{k}} \left\{ e_{1\mathbf{k}} [h_{3\uparrow}^\dagger(\mathbf{k})h_{1\downarrow}^\dagger(-\mathbf{k}) + h_{2\uparrow}^\dagger(\mathbf{k})h_{4\downarrow}^\dagger(-\mathbf{k})] + \text{H. c.} \right\} \\
&+ \sum_{\mathbf{k}} \left\{ e_{2\mathbf{k}} [h_{1\uparrow}^\dagger(\mathbf{k})h_{3\downarrow}^\dagger(-\mathbf{k}) + h_{4\uparrow}^\dagger(\mathbf{k})h_{2\downarrow}^\dagger(-\mathbf{k})] + \text{H. c.} \right\} \\
&+ \sum_{\mathbf{k}} \left\{ f_{1\mathbf{k}} [h_{4\uparrow}^\dagger(\mathbf{k})h_{1\downarrow}^\dagger(-\mathbf{k}) + h_{2\uparrow}^\dagger(\mathbf{k})h_{3\downarrow}^\dagger(-\mathbf{k})] + \text{H. c.} \right\} \\
&+ \sum_{\mathbf{k}} \left\{ f_{2\mathbf{k}} [h_{1\uparrow}^\dagger(\mathbf{k})h_{4\downarrow}^\dagger(-\mathbf{k}) + h_{3\uparrow}^\dagger(\mathbf{k})h_{2\downarrow}^\dagger(-\mathbf{k})] + \text{H. c.} \right\}.
\end{aligned} \tag{A12}$$

In the above expressions, N is the number of unit cells,

$$\begin{aligned}
\epsilon_0 &= -\frac{3}{2}J\bar{s}^2 + 2\xi(1 - \bar{s}^2 + \bar{d}^2 - 2x) - 2\mu(2x - 2\bar{d}^2) \\
&+ J'(Q_x^2 + Q_y^2 - P_x^2 - P_y^2) \\
&+ \frac{3}{2}J(|\Pi_x|^2 + |\Pi_y|^2 + 4|\Delta_x|^2 + 4|\Delta_y|^2) \\
&+ V(2 + 2\bar{d}^2 - 4x) + 8V(1 - x)^2,
\end{aligned}$$

$$\begin{aligned}
A_{\mathbf{k}} &= J'(P_x \cos k_x + P_y \cos k_y), \\
B_{\mathbf{k}} &= -J'(Q_x \cos k_x + Q_y \cos k_y), \\
C_{\mathbf{k}} &= J/4 - \xi,
\end{aligned} \tag{A13}$$

and

$$\begin{aligned}
a_{\mathbf{k}} &= -t, & b_{\mathbf{k}} &= \mu, \\
c_{\mathbf{k}} &= c_{R\mathbf{k}} + ic_{I\mathbf{k}}, & d_{\mathbf{k}} &= d_{R\mathbf{k}} + id_{I\mathbf{k}}, \\
e_{1\mathbf{k}} &= e_{R\mathbf{k}} + ie_{I\mathbf{k}}, & e_{2\mathbf{k}} &= e_{R\mathbf{k}} - ie_{I\mathbf{k}}, \\
f_{1\mathbf{k}} &= f_{R\mathbf{k}} + if_{I\mathbf{k}}, & f_{2\mathbf{k}} &= f_{R\mathbf{k}} - if_{I\mathbf{k}},
\end{aligned} \tag{A14}$$

where

$$\begin{aligned}
c_{R\mathbf{k}} &= -t' \left(\bar{d}^2 - \frac{1}{2} \bar{s}^2 \right) (\cos k_x + \cos k_y) \\
&+ \frac{t'}{2} (P_x \cos k_x + P_y \cos k_y) \\
&- \frac{3}{8} J' (\Pi_x \cos k_x + \Pi_y \cos k_y), \\
c_{I\mathbf{k}} &= -t' \left(\bar{d}^2 + \frac{1}{2} \bar{s}^2 \right) (\sin k_x - \sin k_y) \\
&+ \frac{t'}{2} (-P_x \sin k_x + P_y \sin k_y) \\
&- \frac{3}{8} J' (\Pi_x \sin k_x - \Pi_y \sin k_y), \tag{A15}
\end{aligned}$$

$$\begin{aligned}
d_{R\mathbf{k}} &= -t' \left(\bar{d}^2 - \frac{1}{2} \bar{s}^2 \right) (\cos k_x + \cos k_y) \\
&- \frac{t'}{2} (P_x \cos k_x + P_y \cos k_y) \\
&- \frac{3}{8} J' (\Pi_x \cos k_x + \Pi_y \cos k_y), \\
d_{I\mathbf{k}} &= -t' \left(\bar{d}^2 + \frac{1}{2} \bar{s}^2 \right) (\sin k_x + \sin k_y) \\
&+ \frac{t'}{2} (P_x \sin k_x + P_y \sin k_y) \\
&- \frac{3}{8} J' (\Pi_x \sin k_x + \Pi_y \sin k_y), \tag{A16}
\end{aligned}$$

$$\begin{aligned}
e_{R\mathbf{k}} &= -\sqrt{2} t' \bar{d} \bar{s} (\cos k_x + \cos k_y) \\
&- \frac{3}{4} J' (\Delta_x \cos k_x + \Delta_y \cos k_y), \\
e_{I\mathbf{k}} &= -\frac{3}{4} J' (\Delta_x \sin k_x - \Delta_y \sin k_y), \tag{A17}
\end{aligned}$$

and

$$\begin{aligned}
f_{R\mathbf{k}} &= -\sqrt{2} t' \bar{d} \bar{s} (\cos k_x + \cos k_y) \\
&- \frac{3}{4} J' (\Delta_x \cos k_x + \Delta_y \cos k_y), \\
f_{I\mathbf{k}} &= -\frac{3}{4} J' (\Delta_x \sin k_x + \Delta_y \sin k_y). \tag{A18}
\end{aligned}$$

Of course, the order parameters, P , Q , Π , and Δ , should be determined self-consistently by satisfying the following conditions:

$$\begin{aligned}
P_x &\equiv \langle t_{i\alpha}^\dagger \tau_{i+\hat{x},\alpha} \rangle, \quad Q_x \equiv \langle t_{i\alpha} \tau_{i+\hat{x},\alpha} \rangle, \\
\Pi_x &= \langle h_{1i\alpha}^\dagger h_{3,i-\hat{x},a} \rangle = \langle h_{1i\alpha}^\dagger h_{4,i-\hat{x},a} \rangle \\
&= \langle h_{2i\alpha}^\dagger h_{3,i+\hat{x},a} \rangle = \langle h_{2i\alpha}^\dagger h_{4,i+\hat{x},a} \rangle, \\
\Delta_x &= \langle h_{1i\downarrow} h_{3,i-\hat{x},\uparrow} \rangle = \langle h_{1i\downarrow} h_{4,i-\hat{x},\uparrow} \rangle \\
&= \langle h_{2i\downarrow} h_{3,i+\hat{x},\uparrow} \rangle = \langle h_{2i\downarrow} h_{4,i+\hat{x},\uparrow} \rangle, \tag{A19}
\end{aligned}$$

and similar equations for the y -direction.

As seen in Eq. (A14) and subsequent equations, $c_{\mathbf{k}}$, $d_{\mathbf{k}}$, $e_{\mathbf{k}}$, and $f_{\mathbf{k}}$ are in general complex. In this case it is not easy to

obtain analytic expressions for the h -fermion spectrum. Fortunately, however, it turns out that we can make the following approximations:

$$\begin{aligned}
c_{\mathbf{k}} &\cong c_{R\mathbf{k}}, \quad d_{\mathbf{k}} \cong d_{R\mathbf{k}}, \\
e_{1\mathbf{k}} &\cong e_{R\mathbf{k}}, \quad e_{2\mathbf{k}} \cong e_{R\mathbf{k}}, \\
f_{1\mathbf{k}} &\cong f_{R\mathbf{k}}, \quad f_{2\mathbf{k}} \cong f_{R\mathbf{k}}. \tag{A20}
\end{aligned}$$

The justification for the above approximation will be given in Appendix A 3 where we discuss the physical meaning of the approximation and provide supporting numerical results. For the time being, however, we proceed to derive saddle-point equations by accepting Eq. (A20).

2. Self-consistent saddle-point equations

After the Bogoliubov transformation, the saddle-point Hamiltonian in Eq. (A8) can be written in the following way:

$$\begin{aligned}
H &= N \epsilon_0 + \sum_{\mathbf{k}} \sum_{l=1}^4 [b_{\mathbf{k}} - \Omega_l(\mathbf{k})] \\
&+ \sum_{\mathbf{k}} \sum_{l=1}^4 \Omega_l(\mathbf{k}) \gamma_{l\alpha}^\dagger(\mathbf{k}) \gamma_{l\alpha}(\mathbf{k}) \\
&+ \sum_{\mathbf{k}} \left\{ w_{\eta 1}(\mathbf{k}) \eta_{1\alpha}^\dagger(\mathbf{k}) \eta_{1\alpha}(\mathbf{k}) + \frac{3}{2} [w_{\eta 1}(\mathbf{k}) - C_{\mathbf{k}}] \right\} \\
&+ \sum_{\mathbf{k}} \left\{ w_{\eta 2}(\mathbf{k}) \eta_{2\alpha}^\dagger(\mathbf{k}) \eta_{2\alpha}(\mathbf{k}) + \frac{3}{2} [w_{\eta 2}(\mathbf{k}) - C_{\mathbf{k}}] \right\}, \tag{A21}
\end{aligned}$$

where

$$\begin{aligned}
w_{\eta 1}(\mathbf{k}) &= \sqrt{(C_{\mathbf{k}} + A_{\mathbf{k}})^2 - B_{\mathbf{k}}^2}, \\
w_{\eta 2}(\mathbf{k}) &= \sqrt{(C_{\mathbf{k}} - A_{\mathbf{k}})^2 - B_{\mathbf{k}}^2}, \\
\Omega_1(\mathbf{k}) &= \sqrt{(a_{\mathbf{k}} - b_{\mathbf{k}} + c_{\mathbf{k}} - d_{\mathbf{k}})^2}, \\
\Omega_2(\mathbf{k}) &= \sqrt{(a_{\mathbf{k}} - b_{\mathbf{k}} - c_{\mathbf{k}} + d_{\mathbf{k}})^2}, \\
\Omega_3(\mathbf{k}) &= \sqrt{(a_{\mathbf{k}} + b_{\mathbf{k}} - c_{\mathbf{k}} - d_{\mathbf{k}})^2 + |e_{\mathbf{k}} + f_{\mathbf{k}}|^2}, \\
\Omega_4(\mathbf{k}) &= \sqrt{(a_{\mathbf{k}} + b_{\mathbf{k}} + c_{\mathbf{k}} + d_{\mathbf{k}})^2 + |e_{\mathbf{k}} + f_{\mathbf{k}}|^2}, \tag{A22}
\end{aligned}$$

and we set $c_{\mathbf{k}} = c_{R\mathbf{k}}$, $d_{\mathbf{k}} = d_{R\mathbf{k}}$, $e_{\mathbf{k}} = e_{R\mathbf{k}}$, and $f_{\mathbf{k}} = f_{R\mathbf{k}}$. In the above equations, $\eta_{1\alpha}(\mathbf{k})$ and $\eta_{2\alpha}(\mathbf{k})$ describe two bosonic particles derived from the linear combination of $t_{\alpha}(\mathbf{k})$ and $\tau_{\alpha}(\mathbf{k})$. Similarly, $\gamma_l(\mathbf{k})$ denote four fermionic Bogoliubov quasi-particles obtained from $h_m(\mathbf{k})$ and $h_m^\dagger(-\mathbf{k})$ [$m = 1, 2, 3, 4$].

Now the ground state energy per unit cell is given by

$$\begin{aligned}
\varepsilon_{gr} &= \frac{\langle H \rangle_{gr}}{N} \\
&= \varepsilon_0 + \frac{1}{N} \sum_{\mathbf{k}} \sum_{l=1}^4 (b_{\mathbf{k}} - \Omega_l(\mathbf{k})) \\
&\quad + \frac{1}{N} \sum_{\mathbf{k}} \frac{3}{2} [w_{\eta 1}(\mathbf{k}) - C_{\mathbf{k}}] + \frac{1}{N} \sum_{\mathbf{k}} \frac{3}{2} [w_{\eta 2}(\mathbf{k}) - C_{\mathbf{k}}].
\end{aligned} \tag{A23}$$

The four saddle-point equations for \bar{s} , \bar{d} , ξ , and μ can be obtained by minimizing the ground state energy as follows:

$$\frac{\partial \varepsilon_{gr}}{\partial \xi} = \frac{\partial(\varepsilon_{gr}/J)}{\partial \bar{s}^2} = \frac{\partial \varepsilon_{gr}}{\partial \mu} = \frac{\partial(\varepsilon_{gr}/J)}{\partial \bar{d}^2} = 0, \tag{A24}$$

where

$$\begin{aligned}
\frac{\partial \varepsilon_{gr}}{\partial \xi} &= 5 - 2\bar{s}^2 + 2\bar{d}^2 - 4x \\
&\quad - \frac{3}{2} \frac{1}{N} \sum_{\mathbf{k}} \left[\frac{C_{\mathbf{k}} + A_{\mathbf{k}}}{w_{\eta 1}(\mathbf{k})} + \frac{C_{\mathbf{k}} - A_{\mathbf{k}}}{w_{\eta 2}(\mathbf{k})} \right], \\
\frac{\partial(\varepsilon_{gr}/J)}{\partial \bar{s}^2} &= -\frac{3}{2} - 2\frac{\xi}{J} \\
&\quad + \frac{t'/J}{N} \sum_{\mathbf{k}} (\cos k_x + \cos k_y) \frac{a_{\mathbf{k}} + b_{\mathbf{k}} - c_{\mathbf{k}} - d_{\mathbf{k}}}{\Omega_3(\mathbf{k})} \\
&\quad - \frac{t'/J}{N} \sum_{\mathbf{k}} (\cos k_x + \cos k_y) \frac{a_{\mathbf{k}} + b_{\mathbf{k}} + c_{\mathbf{k}} + d_{\mathbf{k}}}{\Omega_4(\mathbf{k})} \\
&\quad + \sqrt{2} \frac{\bar{d} t'/J}{\bar{s} N} \sum_{\mathbf{k}} (\cos k_x + \cos k_y) \left[\frac{e_{\mathbf{k}} + f_{\mathbf{k}}}{\Omega_3(\mathbf{k})} + \frac{e_{\mathbf{k}} + f_{\mathbf{k}}}{\Omega_4(\mathbf{k})} \right], \\
\frac{\partial \varepsilon_{gr}}{\partial \mu} &= -4(x - \bar{d}^2 - 1) \\
&\quad - \frac{1}{N} \sum_{\mathbf{k}} \left[-\frac{a_{\mathbf{k}} - b_{\mathbf{k}} - c_{\mathbf{k}} + d_{\mathbf{k}}}{\Omega_1(\mathbf{k})} - \frac{a_{\mathbf{k}} - b_{\mathbf{k}} + c_{\mathbf{k}} - d_{\mathbf{k}}}{\Omega_2(\mathbf{k})} \right. \\
&\quad \quad \left. + \frac{a_{\mathbf{k}} + b_{\mathbf{k}} - c_{\mathbf{k}} - d_{\mathbf{k}}}{\Omega_3(\mathbf{k})} + \frac{a_{\mathbf{k}} + b_{\mathbf{k}} + c_{\mathbf{k}} + d_{\mathbf{k}}}{\Omega_4(\mathbf{k})} \right], \\
\frac{\partial(\varepsilon_{gr}/J)}{\partial \bar{d}^2} &= 2\frac{\xi}{J} + 4\frac{\mu}{J} + 2\frac{V}{J} \\
&\quad - \frac{2t'/J}{N} \sum_{\mathbf{k}} (\cos k_x + \cos k_y) \frac{a_{\mathbf{k}} + b_{\mathbf{k}} - c_{\mathbf{k}} - d_{\mathbf{k}}}{\Omega_3(\mathbf{k})} \\
&\quad + \frac{2t'/J}{N} \sum_{\mathbf{k}} (\cos k_x + \cos k_y) \frac{a_{\mathbf{k}} + b_{\mathbf{k}} + c_{\mathbf{k}} + d_{\mathbf{k}}}{\Omega_4(\mathbf{k})} \\
&\quad + \sqrt{2} \frac{\bar{s} t'/J}{\bar{d} N} \sum_{\mathbf{k}} (\cos k_x + \cos k_y) \left[\frac{e_{\mathbf{k}} + f_{\mathbf{k}}}{\Omega_3(\mathbf{k})} + \frac{e_{\mathbf{k}} + f_{\mathbf{k}}}{\Omega_4(\mathbf{k})} \right].
\end{aligned} \tag{A25}$$

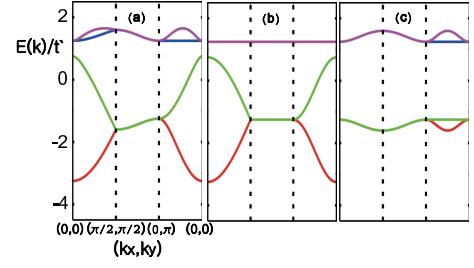


FIG. 6: (Color online) Band structure of the h -fermion at half-filling. (a) The full band structure of the mean-field Hamiltonian, $H_{\text{fermion}} = H_{\text{fermion}}^{(0)} + H_{+,+,-,-} + H_{+,-,-,+}$. (b) The band structure obtained if H_{fermion} is approximated to be $H_{\text{fermion}}^{(0)} + H_{+,+,-,-}$. (c) The additional band structure due to the remaining term, $H_{+,-,-,+}$. For convenience, we plot the band structure of $H_{\text{fermion}}^{(0)} + H_{+,-,-,+}$.

Self-consistency conditions for eight order parameters can also be written in terms of new quasi-particle spectra:

$$\begin{aligned}
P_x &= \frac{3}{4} \frac{1}{N} \sum_{\mathbf{k}} \cos k_x \left[\frac{C_{\mathbf{k}} + A_{\mathbf{k}}}{w_{\eta 1}(\mathbf{k})} - \frac{C_{\mathbf{k}} - A_{\mathbf{k}}}{w_{\eta 2}(\mathbf{k})} \right], \\
Q_x &= -\frac{3}{4} \frac{1}{N} \sum_{\mathbf{k}} \cos k_x \left[\frac{B_{\mathbf{k}}}{w_{\eta 1}(\mathbf{k})} + \frac{B_{\mathbf{k}}}{w_{\eta 2}(\mathbf{k})} \right], \\
\Pi_x &= \frac{1}{4} \frac{1}{N} \sum_{\mathbf{k}} \cos k_x \frac{a_{\mathbf{k}} + b_{\mathbf{k}} - c_{\mathbf{k}} - d_{\mathbf{k}}}{\Omega_3(\mathbf{k})} \\
&\quad - \frac{1}{4} \frac{1}{N} \sum_{\mathbf{k}} \cos k_x \frac{a_{\mathbf{k}} + b_{\mathbf{k}} + c_{\mathbf{k}} + d_{\mathbf{k}}}{\Omega_4(\mathbf{k})}, \\
\Delta_x &= -\frac{1}{8} \frac{1}{N} \sum_{\mathbf{k}} \cos k_x \left[\frac{e_{\mathbf{k}} + f_{\mathbf{k}}}{\Omega_3(\mathbf{k})} + \frac{e_{\mathbf{k}} + f_{\mathbf{k}}}{\Omega_4(\mathbf{k})} \right],
\end{aligned} \tag{A26}$$

and additional four self-consistency conditions for P_y , Q_y , Π_y , and Δ_y are obtained when $\cos k_x$ is replaced by $\cos k_y$.

3. Validity of the approximated h -fermion dispersion

In order to justify the approximations used in Eq.(A20), we start by expressing the fermionic part of the Hamiltonian in terms of the bonding and anti-bonding fermionic operators that can be written as follows:

$$\begin{aligned}
h_{i+a} &\equiv \frac{1}{\sqrt{2}} (h_{1ia} + h_{2ia}), \\
h_{i-a} &\equiv \frac{1}{\sqrt{2}} (h_{1ia} - h_{2ia}), \\
v_{i+a} &\equiv \frac{1}{\sqrt{2}} (h_{3ia} + h_{4ia}), \\
v_{i-a} &\equiv \frac{1}{\sqrt{2}} (h_{3ia} - h_{4ia}),
\end{aligned} \tag{A27}$$

where h_+ and h_- describe the bonding and anti-bonding state for the horizontal dimers, respectively. v_+ and v_- play exactly the same role for the vertical dimers.

The fermionic part of the Hamiltonian can be decomposed into three parts:

$$H_{\text{fermion}} = H_{\text{fermion}}^{(0)} + H_{++,-} + H_{+,-,+}, \quad (\text{A28})$$

where

$$\begin{aligned} H_{\text{fermion}}^{(0)} = & \sum_{\mathbf{k}} a_{\mathbf{k}} \left[h_{+a}^{\dagger}(\mathbf{k}) h_{+a}(\mathbf{k}) - h_{-a}^{\dagger}(\mathbf{k}) h_{-a}(\mathbf{k}) \right. \\ & \left. + v_{+a}^{\dagger}(\mathbf{k}) v_{+a}(\mathbf{k}) - v_{-a}^{\dagger}(\mathbf{k}) v_{-a}(\mathbf{k}) \right] \\ & + \sum_{\mathbf{k}} b_{\mathbf{k}} \left[h_{+a}^{\dagger}(\mathbf{k}) h_{+a}(\mathbf{k}) + h_{-a}^{\dagger}(\mathbf{k}) h_{-a}(\mathbf{k}) \right. \\ & \left. + v_{+a}^{\dagger}(\mathbf{k}) v_{+a}(\mathbf{k}) + v_{-a}^{\dagger}(\mathbf{k}) v_{-a}(\mathbf{k}) \right], \end{aligned} \quad (\text{A29})$$

$$\begin{aligned} H_{++,-} = & \sum_{\mathbf{k}} c_{R\mathbf{k}} \left[h_{+a}^{\dagger}(\mathbf{k}) v_{+a}(\mathbf{k}) + v_{+a}^{\dagger}(\mathbf{k}) h_{+a}(\mathbf{k}) \right. \\ & \left. + h_{-a}^{\dagger}(\mathbf{k}) v_{-a}(\mathbf{k}) + v_{-a}^{\dagger}(\mathbf{k}) h_{-a}(\mathbf{k}) \right] \\ & + \sum_{\mathbf{k}} d_{R\mathbf{k}} \left[h_{+a}^{\dagger}(\mathbf{k}) v_{+a}(\mathbf{k}) + v_{+a}^{\dagger}(\mathbf{k}) h_{+a}(\mathbf{k}) \right. \\ & \left. - h_{-a}^{\dagger}(\mathbf{k}) v_{-a}(\mathbf{k}) - v_{-a}^{\dagger}(\mathbf{k}) h_{-a}(\mathbf{k}) \right] \\ & + \sum_{\mathbf{k}} \left\{ e_{R\mathbf{k}} [v_{+\uparrow}^{\dagger}(\mathbf{k}) h_{+\downarrow}^{\dagger}(-\mathbf{k}) + h_{+\uparrow}^{\dagger}(\mathbf{k}) v_{+\downarrow}^{\dagger}(-\mathbf{k}) \right. \\ & \left. + v_{+\uparrow}^{\dagger}(\mathbf{k}) h_{+\downarrow}^{\dagger}(-\mathbf{k}) + h_{+\uparrow}^{\dagger}(\mathbf{k}) v_{+\downarrow}^{\dagger}(-\mathbf{k}) \right] + \text{H. c.} \left. \right\} \\ & + \sum_{\mathbf{k}} \left\{ f_{R\mathbf{k}} [v_{+\uparrow}^{\dagger}(\mathbf{k}) h_{+\downarrow}^{\dagger}(-\mathbf{k}) + h_{+\uparrow}^{\dagger}(\mathbf{k}) v_{+\downarrow}^{\dagger}(-\mathbf{k}) \right. \\ & \left. - v_{-\uparrow}^{\dagger}(\mathbf{k}) h_{-\downarrow}^{\dagger}(-\mathbf{k}) - h_{-\uparrow}^{\dagger}(\mathbf{k}) v_{-\downarrow}^{\dagger}(-\mathbf{k}) \right] + \text{H. c.} \left. \right\}, \end{aligned} \quad (\text{A30})$$

and

$$\begin{aligned} H_{+,-,+} = & \sum_{\mathbf{k}} ic_{I\mathbf{k}} \left[v_{-a}^{\dagger}(\mathbf{k}) h_{+a}(\mathbf{k}) - h_{+a}^{\dagger}(\mathbf{k}) v_{-a}(\mathbf{k}) \right. \\ & \left. + v_{+a}^{\dagger}(\mathbf{k}) h_{-a}(\mathbf{k}) - h_{-a}^{\dagger}(\mathbf{k}) v_{+a}(\mathbf{k}) \right] \\ & + \sum_{\mathbf{k}} id_{I\mathbf{k}} \left[v_{+a}^{\dagger}(\mathbf{k}) h_{-a}(\mathbf{k}) - h_{-a}^{\dagger}(\mathbf{k}) v_{+a}(\mathbf{k}) \right. \\ & \left. + h_{+a}^{\dagger}(\mathbf{k}) v_{-a}(\mathbf{k}) - v_{-a}^{\dagger}(\mathbf{k}) h_{+a}(\mathbf{k}) \right] \\ & + \sum_{\mathbf{k}} \left\{ ie_{I\mathbf{k}} [v_{-\uparrow}^{\dagger}(\mathbf{k}) h_{+\downarrow}^{\dagger}(-\mathbf{k}) - h_{+\uparrow}^{\dagger}(\mathbf{k}) v_{-\downarrow}^{\dagger}(-\mathbf{k}) \right. \\ & \left. + v_{+\uparrow}^{\dagger}(\mathbf{k}) h_{-\downarrow}^{\dagger}(-\mathbf{k}) - h_{-\uparrow}^{\dagger}(\mathbf{k}) v_{+\downarrow}^{\dagger}(-\mathbf{k}) \right] + \text{H. c.} \left. \right\} \\ & + \sum_{\mathbf{k}} \left\{ if_{I\mathbf{k}} [v_{+\uparrow}^{\dagger}(\mathbf{k}) h_{-\downarrow}^{\dagger}(-\mathbf{k}) - h_{-\uparrow}^{\dagger}(\mathbf{k}) v_{+\downarrow}^{\dagger}(-\mathbf{k}) \right. \\ & \left. + h_{+\uparrow}^{\dagger}(\mathbf{k}) v_{-\downarrow}^{\dagger}(-\mathbf{k}) - v_{-\uparrow}^{\dagger}(\mathbf{k}) h_{+\downarrow}^{\dagger}(-\mathbf{k}) \right] + \text{H. c.} \left. \right\}, \end{aligned} \quad (\text{A31})$$

where it is important to note that $H_{++,-}$ describes the fermion hopping and pairing processes within the band of the same bonding character. On the other hand, $H_{+,-,+}$ contains mixing processes between the bonding and anti-bonding bands. The approximation used in Eq.(A20) corresponds to the omission of $H_{+,-,+}$ from H_{fermion} .

To judge the validity of this approximation, let us first consider the effect of hopping terms alone from the Hamiltonian. In Fig. 6 (a) we plot the full band structure of H_{fermion} at half filling. Since the unit cell consists of four spins, there are four bands. The two bands lying high in energy are almost flat while the other two are dispersive. In Fig. 6 (b) we show the band structure obtained when H_{fermion} is approximated to be $H_{\text{fermion}}^{(0)} + H_{++,-}$. As one can see, the difference between the full and the approximated band structure is minor. The almost flat two bands in the full Hamiltonian, which are high in energy and so do not play important roles at small hole doping, become completely localized. The shapes of the other two dispersive bands are only slightly modified. Now, to explicitly demonstrate the minor influence of the remaining part, i.e., $H_{+,-,+}$, we consider an extreme situation where the role of $H_{+,-,+}$ is maximized. That is, we consider the band structure of $H_{\text{fermion}}^{(0)} + H_{+,-,+}$. As seen in Fig. 6 (c), the resulting band structure is almost featureless. Thus, the main effect of $H_{+,-,+}$ would be providing only a weak distortion to the bands of $H_{++,-}$.

Since normal mixing between the bands with different bonding characters generates minor effects, it is reasonable to assume that the pairing process between different bonding bands also does not modify the band structure significantly. It can be further argued that these results are valid also for the case of finite doping because the fermionic band structure has similar structure to the half-filled case as can be seen in Eq. (A22) and there is no level crossing upon doping. In conclusion, we believe that the approximation used in Eq.(A20) is accurate enough to capture the essential physics while it renders convenient simplification in calculations.

-
- * Electronic address: kpark@kias.re.kr
- ¹ S. Sachdev, *Rev. Mod. Phys.* **75**, 913 (2003).
 - ² S. A. Kivelson, I. P. Bindloss, E. Fradkin, V. Oganesyan, J. M. Tranquada, A. Kapitulnik, and C. Howald, *Rev. Mod. Phys.* **75**, 1201 (2003).
 - ³ P. A. Lee, N. Nagaosa, and X.-G. Wen, *Rev. Mod. Phys.* **78**, 17 (2006).
 - ⁴ H. Kageyama, K. Yoshimura, R. Stern, N. V. Mushnikov, K. Onizuka, M. Kato, K. Kosuge, C. P. Slichter, T. Goto, and Y. Ueda, *Phys. Rev. Lett.* **82**, 3168 (1999).
 - ⁵ Z. Hiroi, M. Hanawa, N. Kobayashi, M. Nohara, H. Takagi, Y. Kato, and M. Takigawa, *J. Phys. Soc. Jpn.* **70**, 3377 (2001).
 - ⁶ J. S. Helton, K. Matan, M. P. Shores, E. A. Nytko, B. M. Bartlett, Y. Yoshida, Y. Takano, A. Suslov, Y. Qiu, J.-H. Chung, D. G. Nocera, and Y. S. Lee, *Phys. Rev. Lett.* **98**, 107204 (2007).
 - ⁷ Y. Okamoto, M. Nohara, H. Aruga-Katori, and H. Takagi, *arXiv:0705.2821* (2007).
 - ⁸ Y. Shimizu, K. Miyagawa, K. Kanoda, M. Maesato, and G. Saito, *Phys. Rev. Lett.* **91**, 107001 (2003).
 - ⁹ K. Kodama, M. Takigawa, M. Horvati, C. Berthier, H. Kageyama, Y. Ueda, S. Miyahara, F. Becca, and F. Mila, *Science* **298**, 395 (2002).
 - ¹⁰ B. D. Gaulin, S. H. Lee, S. Haravifard, J. P. Castellan, A. J. Berlinsky, H. A. Dabkowska, Y. Qiu, and J. R. D. Copley, *Phys. Rev. Lett.* **93**, 267202 (2004).
 - ¹¹ B. S. Shastry and B. Sutherland, *Physica B* **108**, 1069 (1981).
 - ¹² M. Albrecht and F. Mila, *Europhys. Lett.* **34**, 145 (1996).
 - ¹³ S. Miyahara and K. Ueda, *Phys. Rev. Lett.* **82**, 3701 (1999).
 - ¹⁴ Z. Weihong, C. J. Hamer, and J. Oitmaa, *Phys. Rev. B* **60**, 6608 (1999); W. Zheng, J. Oitmaa, and C. J. Hamer, *ibid.* **65**, 014408 (2001).
 - ¹⁵ E. Müller-Hartmann, R. R. P. Singh, C. Knetter, and G. S. Uhrig, *Phys. Rev. Lett.* **84**, 1808 (2000).
 - ¹⁶ A. Koga and N. Kawakami, *Phys. Rev. Lett.* **84**, 4461 (2000).
 - ¹⁷ A. Läuchli, S. Wessel, and M. Sigrist, *Phys. Rev. B* **66**, 014401 (2002).
 - ¹⁸ C. H. Chung, J. B. Marston, and S. Sachdev, *Phys. Rev. B* **64**, 134407 (2001).
 - ¹⁹ K. Park and S. Sachdev, *Phys. Rev. B* **64**, 184510 (2001).
 - ²⁰ S. Sachdev and R. N. Bhatt, *Phys. Rev. B* **41**, 9323 (1990).
 - ²¹ K. Park, *Phys. Rev. B* **67**, 094513 (2003).
 - ²² K. Park and S. Sachdev, *cond-mat/0104519*.
 - ²³ B. S. Shastry and B. Kumer, *Prog. Theor. Phys. Supplement* **145**, 1 (2002).
 - ²⁴ C. H. Chung and Y. B. Kim, *Phys. Rev. Lett.* **93**, 207004 (2004).
 - ²⁵ J. Liu, N. Trivedi, Y. Lee, B. N. Harmon, and J. Schmalian, *cond-mat/0702118*.
 - ²⁶ R. B. Laughlin, *Phys. Rev. Lett.* **80**, 5188 (1998).
 - ²⁷ S. Sachdev, *Physica A* **313**, 252 (2002).
 - ²⁸ M. Vojta, Y. Zhang, and S. Sachdev, *Phys. Rev. B* **62**, 6721 (2000).
 - ²⁹ P. W. Leung and Y. F. Cheng, *Phys. Rev. B* **69**, 180403(R), (2004).
 - ³⁰ S. Haravifard, S. R. Dunsiger, S. El Shawish, B. D. Gaulin, H. A. Dabkowska, M. T. F. Telling, T. G. Perring, and J. Bonca, *Phys. Rev. Lett.* **97**, 247206 (2006).